expressivity among these individuals with doubly heterozygous mutations of *BMP4* and *OTX2* could be attributed to the functionally related roles of the two genes observed in animal models. Both *Otx2* and *Bmp4* are involved in retinal pigment epithelial differentiation and formation of the anterior structures of the eyes in vertebrates [8]. Co-expression of the two genes was observed in some species [9]. Here, we present a patient with concurrent deletion of *OTX2* and *BMP4* that lends support to the aforementioned hypothesis, and to better delineate, in further detail, the phenotypic characteristics of the 14q22 microdeletion syndrome.

2. Clinical report

The propositus is a Japanese girl born to non-consanguineous parents. Her family history was non-contributory. The pregnancy was uneventful and she was born at 37 and 5/7 weeks of gestation via cesarean section for decreased fetal movements. Her birth weight was 2335 g and head circumference was 33 cm. She had a wide open anterior fontanelle measuring approximately 3 × 3 cm. Her face was characterized by a prominent forehead, microphthalmia, thin upper lip, long palpebral fissures, and long eyelashes (Fig. 1-A). Ophthalmic slit-lamp examination revealed bilateral extreme microcornea with a corneal diameter of 4 mm in the right eye and 2 mm in the left eye, severe anterior segment dysgenesis with bilateral corneal opacities, iris coloboma in the right eye, and occluded pupil in the left eye (Fig. 1-B). No posterior segment abnormalities were identified in either eye by ultrasonography. Both eyes showed light perception, but grating visual acuity could not be measured. Involuntary upward movements of the eye were seen on both sides. There was a prominent finger pad and a small but deep sacral dimple. She also had a small atrial septal defect, which closed spontaneously. She showed delayed tooth eruption. At two weeks of age, a computed tomography of the head revealed only an extremely thin corpus callosum without significant cerebral volume changes (Fig. 1-C). A magnetic resonance imaging at the age of 21 months demonstrated significant and progressive global atrophy, most prominent in the frontal lobes. The striking volume loss predominantly involved the white matter, with relative preservation of the gray matter (Fig. 1-D). Neuroimaging did not reveal any suprasellar abnormalities. Her thyroid function test results were all within normal limits (thyroid-stimulating hormone 4.28 mU/L (reference for age: 0.7–6.4 mIU/L); free triiodothyronine 4.1 pg/mL (2.3–5.6 pg/mL); free thyroxine1.2 ng/dL (0.8–2.2 ng/dL)). Serum somatomedin C was normal for age. i.e., 93.0 ng/mL (74–202 ng/mL). Her development was profoundly delayed despite the absence of microcephaly, failure to thrive, or deafness on auditory brainstem response. Currently, she is 2 years and 10 months old and her height is 85.7 cm (−1.35SD), weight is 10.34 kg (−1.64SD), and head circumference is 48.4 cm (+0.08SD). She is only able to sit without support. She does not follow commands or

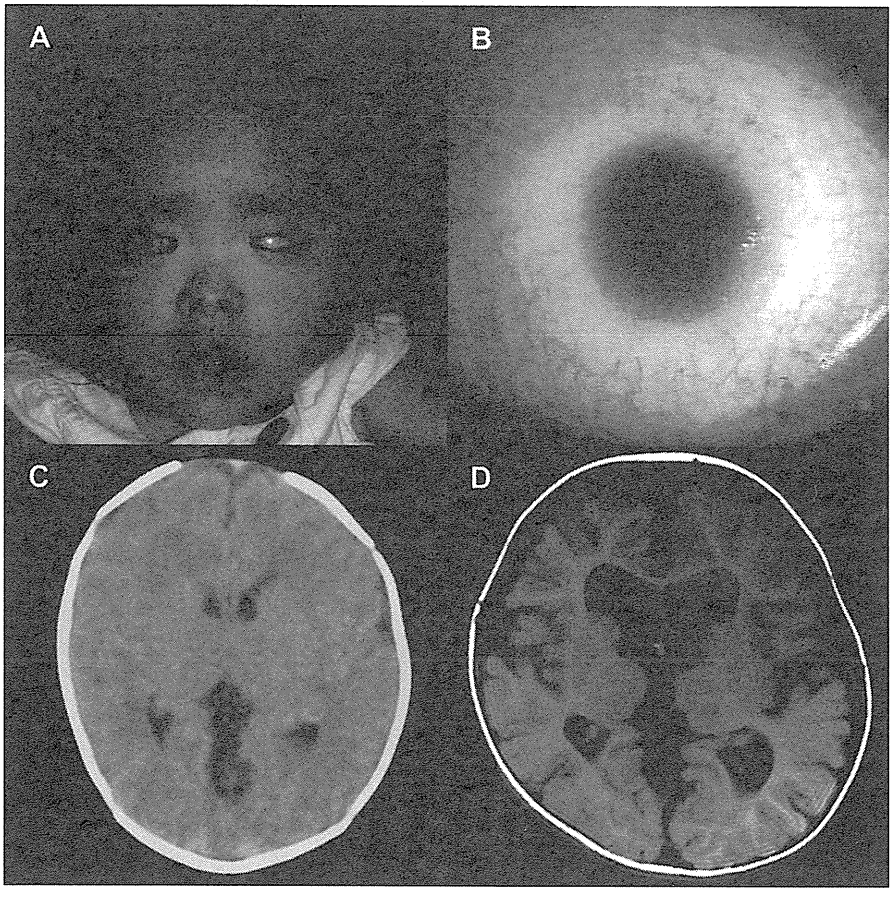

Fig. 1. Clinical and radiographic features of the propositus. A: Facial appearance of the propositus. Note the prominent forehead, microphthalmia, thin upper lip, long palpebral fissures, and long eyelashes, B: Appearance of the left eye at the age of 2 years: extreme microcornea with an occluded pupil can be seen. C: Axial computed tomography at 2 weeks of age. Note the preserved white matter volume. D: Axial magnetic resonance imaging of the brain at 21 months of age, demonstrating significant global volume loss predominantly involving white matter.

speak any meaningful words. She has never had seizures. On examination, she has bilateral microphthalmia, and diffuse hypotonia. There are no dystonic movements or diurnal fluctuations in her muscle tone. A G-band analysis was reportedly normal. A microarray analysis demonstrated a de novo 6.2-Mb deletion in 14q22.2-22.1 from position 52,830,547 to 59, 031,284 (NCBI36/hg18, March 2006), which included approximately 53 genes (Fig. 2).

3. Discussion

Here, we report a patient with severe anterior segment dysgenesis due to concurrent heterozygous deletion involving both the *OTX2* and *BMP4* loci. A review of the previously reported patients with concurrent deletion of *OTX2* and *BMP4*, i.e. [1], Case 1 and 2 in Ref. [4] reveals that the severe AM phenotype indeed showed high penetrance: all three patients with such concurrent deletion showed severe AM. Our clinical observation is compatible with the notion that BMP4 and OTX2 act via a common pathway.

It is intriguing that two functionally close genes such as *BMP4* and *OTX2* are in physical proximity to each other. Another example of functional proximity between two neighboring genes has been reported for the combination of *EVC* and *EVC2* at the Ellis-van Creveld syndrome (MIM 225500) locus: mutations in the two genes, which share no sequence homology, lead to the same syndromic phenotype [10]. It is speculated that the two genes, namely, *EVC* and *EVC2*, are under the control of the same regulatory element, and a similar explanation could apply to the combination of *BMP4* and *OTX2*. Phylogenetic analysis of the alignment of *Bmp4* and *Otx2* reveals that the proximity of the two genes is conserved down to the chicken. This genomic observation does not prove, but lends support to the idea that the alignment of the two genes in proximity may be advantageous from an evolutionary standpoint. Alternatively, *OTX2* and *BMP4* may not have any functional complementarity despite their physical proximity, since *Otx2* interacts with *Sox2*, whereas *Bmp4* interacts with *Pax6* and *Bmp7* in lens formation [11].

We confirmed that AM represents a cardinal sign of the 14q22 microdeletion syndrome. In order to define 14q22 microdeletion syndrome as a clinically recognizable entity, we further attempted to delineate the extra-ocular phenotypes in patients with 14q22 microdeletion. At least seven out of thirteen patients with microdeletion involving 14q22 showed decreased white matter volume or increased ventricular size at some point in their clinical course [1,12]:, case 1 and 2 in Ref. [4], III-5 and III-6 in Ref. [13] and the propositus.

Inclusion mapping among patients with 14q22 microdeletion suggests that the shortest region of overlap for decreased white matter volume is located between the centromeric end of the deletion interval of the propositus and the telomeric end of the deletion interval reported by Hayashi et al. (Fig. 3) [12]. Exclusion mapping with Case 1 described in the report by Wyatt et al., who had no abnormal findings on computed tomography findings, indicated *BMP4* as the only candidate gene for the white matter lesion [14]. However, intragenic loss-of-function mutations in *BMP4* have been reported to cause ophthalmic lesions without exerting any effect on the white matter [15]. Lumaka et al. described a family with microscopic deletions involving *BMP4*, and only half of affected members had brain lesions [13]. A possible explanation for this inconsistency in the mappings is that decreased white matter volume associated with 14q22 microdeletion could be an age-dependent lesion. Indeed, serial neuroimaging in the propositus showed normal white matter volume at 2 weeks of age, but a striking progressive white matter loss at 21 months of age. We suggest that serial neuroimaging be performed in other patients with 14q22 microdeletion to confirm whether the decreased white matter volume associated with 14q22 microdeletion might be age-dependent and progressive. If so, the above mapping data require some modification.

From the genetic counseling standpoint, it is critical to investigate the exact etiology of AM. 14q22 microdeletion syndrome, which is essentially a de novo condition, carries a low risk of recurrence, whereas the risk can be as high as 25% in other autosomal recessive conditions [16]. In conclusion, 14q22 microdeletion should be included in the differential diagnosis of patients presenting with anterior segment dysgenesis of the eyes, and decreased white matter volume on brain imaging may be helpful for the clinical diagnosis.

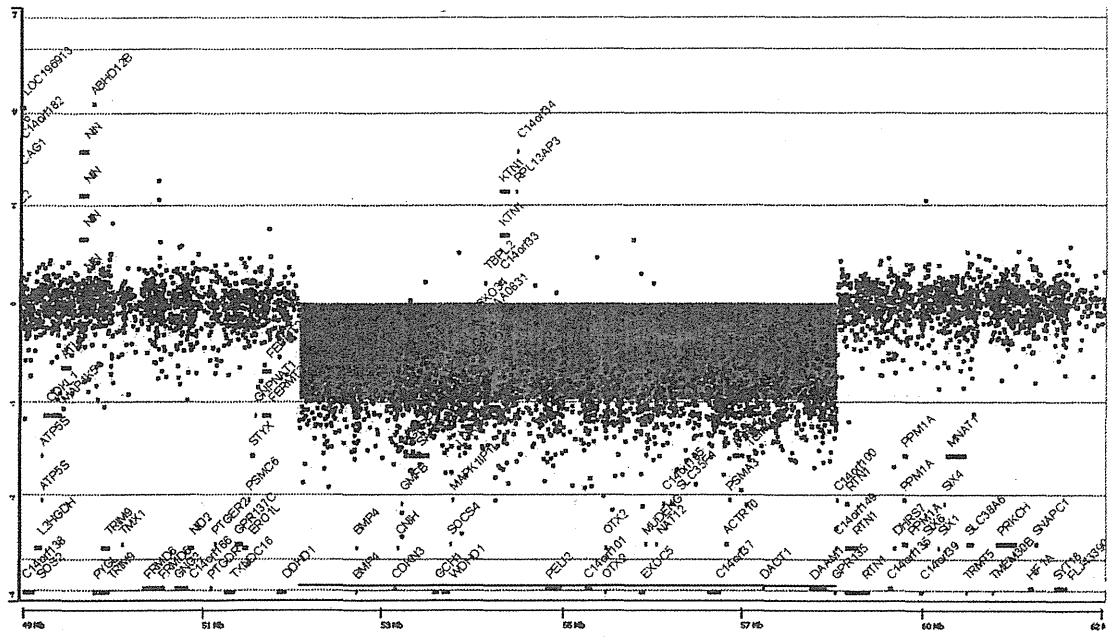

Fig. 2. Result of the microarray analysis. Note the deleted region highlighted in green.

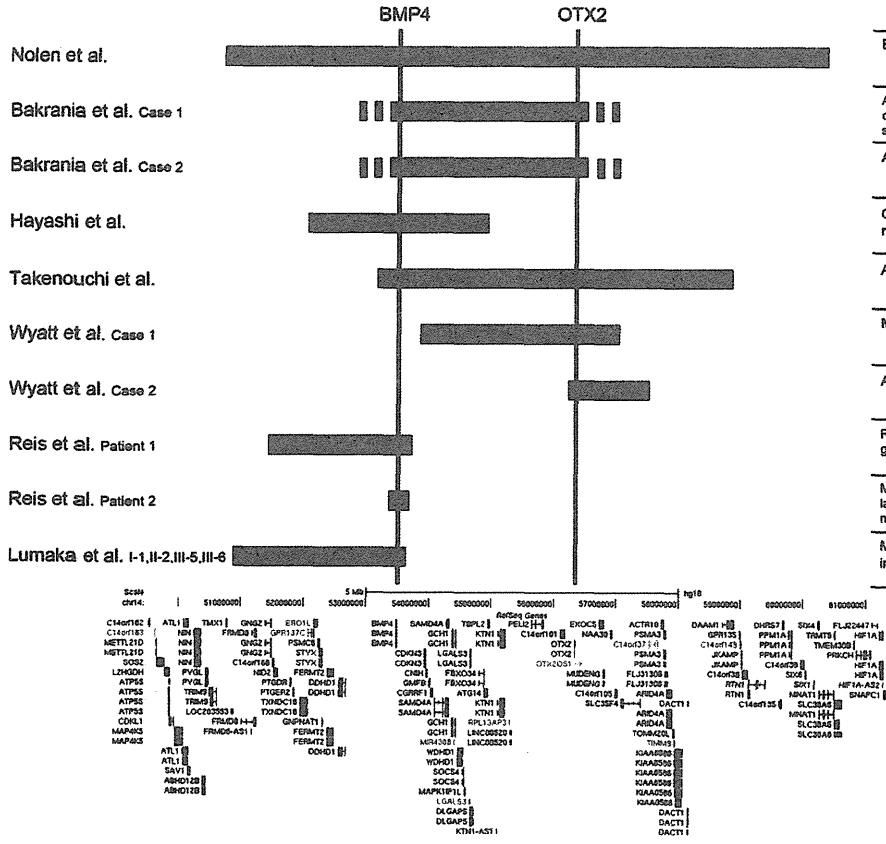

Eye(s)	Neuroimaging
Bilateral fused eyelids	Thin corpus callosum, global reduction of white matter at 6months, absence of the anterior pituitary gland at 2 years
Anophthalmia, sclerocornea (right), coloboma (left), optic nerve hypoplasia, no light perception	Partial agenesis of corpus callosum and hypoplasia of inferior cerebellar vermis, lateral ventricles mildly prominent
Anophthalmia	Partial cerebellar vermis hypoplasia, generalized lack of white matter
Congenital glaucoma, sclerocornea	Decreased white matter, lateral ventricle dilatation
Anterior segment dysgenesis	Progressive white matter loss at 21months
Microphthalmia	Normal
Anophthalmia	(Skull fracture and subdural hematoma)
Rieger anomaly, congenital glaucoma, microcornea, nystagmus	Normal
Microphthalmia, persistence of pupillary membrane, high myopia, strabismus, nystagmus, corectopia (right)	Not performed
Microphthalmia and sclerocornea in III-6	Mild bilateral white matter lesions in III-6 and ventricular dilatation in III-5

Fig. 3. Schematic mapping of patients with 14q22 microdeletion. The black vertical lines represent the extent of deletion on the UCSC genome browser (http://genome.ucsc.edu/) (NCBI36/hg18, March 2006) in each patient, whose ocular and neuroimaging characteristics are listed on the right.

References

[1] L.D. Nolen, D. Amor, A. Haywood, L. St Heaps, C. Willcock, M. Mihelec, P. Tam, F. Billson, J. Grigg, G. Peters, R.V. Jamieson, Deletion at 14q22-23 indicates a contiguous gene syndrome comprising anophthalmia, pituitary hypoplasia, and ear anomalies, Am. J. Med. Genet. A 140 (2006) 1711–1718.

[2] F. Muller, H. Rohrer, A. Vogel-Hopker, Bone morphogenetic proteins specify the retinal pigment epithelium in the chick embryo, Development 134 (2007) 3483–3493.

[3] J.R. Martinez-Morales, M. Signore, D. Acampora, A. Simeone, P. Bovolenta, Otx genes are required for tissue specification in the developing eye, Development 128 (2001) 2019–2030.

[4] P. Bakrania, M. Efthymiou, J.C. Klein, A. Salt, D.J. Bunyan, A. Wyatt, C.P. Ponting, A. Martin, S. Williams, V. Lindley, J. Gilmore, M. Restori, A.G. Robson, M.M. Neveu, G.E. Holder, J.R. Collin, D.O. Robinson, P. Farndon, H. Johansen-Berg, D. Gerrelli, N.K. Ragge, Mutations in BMP4 cause eye, brain, and digit developmental anomalies: overlap between the BMP4 and hedgehog signaling pathways, Am. J. Hum. Genet. 82 (2008) 304–319.

[5] N.K. Ragge, A.G. Brown, C.M. Poloschek, B. Lorenz, R.A. Henderson, M.P. Clarke, I. Russell-Eggitt, A. Fielder, D. Gerrelli, J.P. Martinez-Barbera, P. Ruddle, J. Hurst, J.R. Collin, A. Salt, S.T. Cooper, P.J. Thompson, S.M. Sisodiya, K.A. Williamson, D.R. Fitzpatrick, V. van Heyningen, I.M. Hanson, Heterozygous mutations of OTX2 cause severe ocular malformations, Am. J. Hum. Genet. 76 (2005) 1008–1022.

[6] B. Chang, R.S. Smith, M. Peters, O.V. Savinova, N.L. Hawes, A. Zabaleta, S. Nusinowitz, J.E. Martin, M.L. Davisson, C.L. Cepko, B.L. Hogan, S.W. John, Haploinsufficient Bmp4 ocular phenotypes include anterior segment dysgenesis with elevated intraocular pressure, BMC Genet. 2 (2001) 18.

[7] I. Matsuo, S. Kuratani, C. Kimura, N. Takeda, S. Aizawa, Mouse Otx2 functions in the formation and patterning of rostral head, Genes Dev. 9 (1995) 2646–2658.

[8] J.R. Martinez-Morales, I. Rodrigo, P. Bovolenta, Eye development: a view from the retina pigmented epithelium, Bioessays 26 (2004) 766–777.

[9] L.S. Gammill, H. Sive, Coincidence of otx2 and BMP4 signaling correlates with Xenopus cement gland formation, Mech. Dev. 92 (2000) 217–226.

[10] S.W. Tompson, V.L. Ruiz-Perez, H.J. Blair, S. Barton, V. Navarro, J.L. Robson, M.J. Wright, J.A. Goodship, Sequencing EVC and EVC2 identifies mutations in two-thirds of Ellis-van Creveld syndrome patients, Hum. Genet. 120 (2007) 663–670.

[11] A.M. Slavotinek, Eye development genes and known syndromes, Mol. Genet. Metab. 104 (2011) 448–456.

[12] S. Hayashi, N. Okamoto, Y. Makita, A. Hata, I. Imoto, J. Inazawa, Heterozygous deletion at 14q22.1-q22.3 including the BMP4 gene in a patient with psychomotor retardation, congenital corneal opacity and feet polysyndactyly, Am. J. Med. Genet. A 146A (2008) 2905–2910.

[13] A. Lumaka, C. Van Hole, I. Casteels, E. Ortibus, V. De Wolf, J.R. Vermeesch, T. Lukusa, K. Devriendt, Variability in expression of a familial 2.79 Mb microdeletion in chromosome 14q22.1-22.2, Am. J. Med. Genet. A 158A (2012) 1381–1387.

[14] A. Wyatt, P. Bakrania, D.J. Bunyan, R.J. Osborne, J.A. Crolla, A. Salt, C. Ayuso, R. Newbury-Ecob, Y. Abou-Rayyah, J.R. Collin, D. Robinson, N. Ragge, Novel heterozygous OTX2 mutations and whole gene deletions in anophthalmia, microphthalmia and coloboma, Hum. Mutat. 29 (2008) E278–E283.

[15] L.M. Reis, R.C. Tyler, K.F. Schilter, O. Abdul-Rahman, J.W. Innis, B.A. Kozel, A.S. Schneider, T.M. Bardakjian, E.J. Lose, D.M. Martin, U. Broeckel, E.V. Semina, BMP4 loss-of-function mutations in developmental eye disorders including SHORT syndrome, Hum. Genet. 130 (2011) 495–504.

[16] T. Bardakjian, A. Weiss, A. Schneider, Anophthalmia/microphthalmia overview, in: R.A. Pagon, T.D. Bird, C.R. Dolan, K. Stephens (Eds.), GeneReviews [Internet], University of Washington, Seattle, Seattle (WA), 1993.

sue in concentric layers, and (5) external loose connective tissue with fibroadipose elements, muscle, and blood vessels. Our patient had each of these elements.

Conservative treatment includes observation with aspiration as needed. In recalcitrant cases not amenable to aspiration or if considerable facial dysmorphism exists, excision is conventionally undertaken.

In summary, congenital cystic eye is exceedingly rare. Diagnosis historically was based on physical and histopathological findings. However, newer imaging modalities are revealing characteristic findings of the condition at or even prior to birth, as in our case. Given the frequent association with intracranial abnormalities, including the possibility of septo-optic dysplasia, neuroimaging is warranted to screen for such aberrations. Finally, although not always required, treatment conventionally involves excision.

James R. Singer, DO
Patrick J. Droste, MS, MD
Adam S. Hassan, MD

Author Affiliations: Metro Health Hospital, Wyoming, Michigan (Singer); Department of Neurology and Ophthalmology, Michigan State University, East Lansing (Singer, Droste, Hassan); Helen DeVos Children's Hospital, Grand Rapids, Michigan (Droste, Hassan).

Corresponding Author: Dr Singer, Metro Health Hospital, 2221 Health Dr SW, Ste 1100, Wyoming, MI 49519 (james-singer@hotmail.com).

Published Online: June 27, 2013.
doi:10.1001/jamaophthalmol.2013.328.

Conflict of Interest Disclosures: None reported.

1. Chaudhry IA, Shamsi FA, Elzaridi E, Arat YO, Riley FC. Congenital cystic eye with intracranial anomalies: a clinicopathologic study. *Int Ophthalmol*. 2007;27(4):223-233.

2. Robb RM, Anthony DC. Congenital cystic eye: recurrence after initial surgical removal. *Ophthalmic Genet*. 2003;24(2):117-123.

3. Tsitouridis I, Michaelides M, Tsantiridis C, Spyridi S, Arvanity M, Efstratiou I. Congenital cystic eye with multiple dermal appendages and intracranial congenital anomalies. *Diagn Interv Radiol*. 2010;16(2):116-121.

4. Gupta R, Seith A, Guglani B, Jain TP. Congenital cystic eye: features on MRI. *Br J Radiol*. 2007;80(955):e137-e140.

5. Pasquale LR, Romayananda N, Kubacki J, Johnson MH, Chan GH. Congenital cystic eye with multiple ocular and intracranial anomalies. *Arch Ophthalmol*. 1991;109(7):985-987.

Development of a Premacular Vitreous Pocket

The premacular vitreous pocket (PVP), or vitreoschisis cavity, is a liquefied vitreous cavity in front of the posterior retina that is characteristic of various macular diseases, including macular holes and diabetic maculopathy.[1] The reason for the development of PVPs is unknown because of the difficulty observing the formed vitreous in vivo. India ink and the fluorescein staining technique have delineated the structure of the PVP in the vitreous cavity in human eyes at autopsy[2]; however, the technique is limited because of the presence of artifacts during fixation of the fragile and mobile vitreous and postmortem changes. Optical coherence tomography has facilitated observation of the vitreous structures in vivo. Herein, we describe the development and fine details of PVPs in real time.

Figure 1. Age-Dependent Changes in Premacular Vitreous Pockets

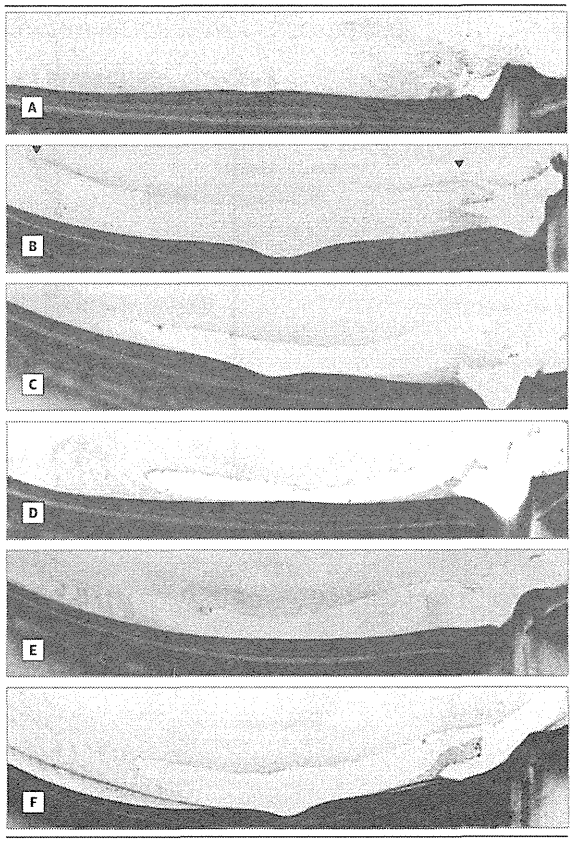

A, No premacular vitreous pocket is seen in the eye of a 2-year-old boy. B, A premacular crack in the formed vitreous (arrowheads) is seen in the eye of a 3-year-old girl, and the Cloquet canal is connected to the crack. Premacular vitreous pockets are seen in the eyes of an 8-year-old boy (C), a 13-year-old boy (D), a 30-year-old man (E), and a 54-year-old woman (F), and they are all connected to the Cloquet canal. F, A partial posterior vitreous detachment is seen in the eye of a 54-year-old woman.

Methods | We retrospectively analyzed the posterior vitreous, retinas, and optic discs of 56 healthy eyes (39 patients; age range, 1-54 years) using swept-source optical coherence tomography (Topcon), which provides detailed images of the fine ocular structures. The scanning protocol used in this study was a single-line scan with 96 overlapping images and a radial scan with 32 overlapping images. Each line has a 12-mm transverse scanning length with 1024-pixel resolution. Eyes that appeared healthy were excluded if the patient had a family history of a hereditary vitreoretinal disease.

Results | A PVP (**Figure 1**C-F) was detected in all eyes of patients older than 10 years and in no eyes of patients younger than 2 years (Figure 1A). A crack in the formed vitreous (Figure 1B), considered to be a primitive structure of the PVP, developed first in eyes around age 2 years. Between ages 3 and

Figure 2. Multifocal Premacular Vitreous Pockets (PVPs) and Temporal Remnants of Regressed Hyaloid Vessels With a PVP

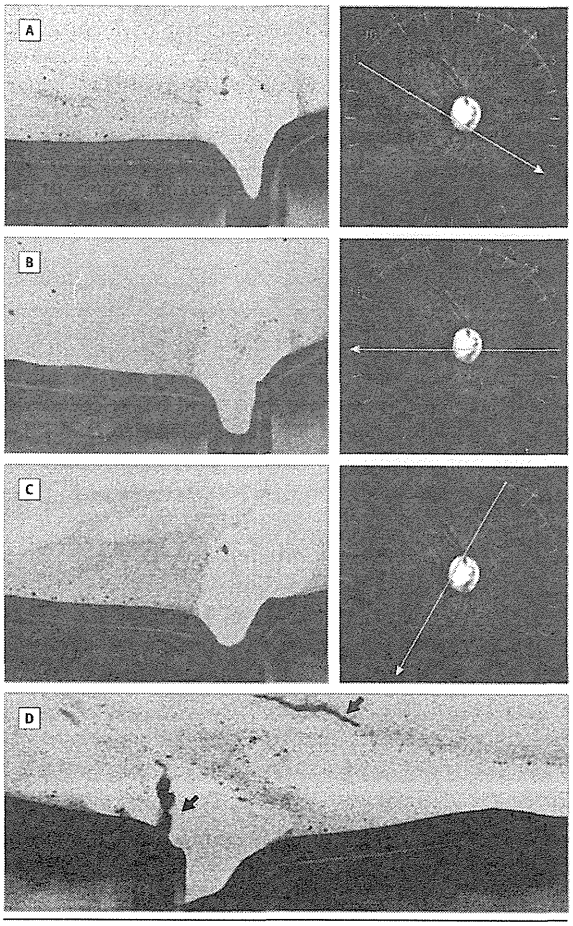

A-C, Sequential radial sections of the temporal premacular vitreous centered on the optic disc in the eye of a 6-year-old boy. Primitive PVPs are seen superotemporally (A) and inferotemporally (C) but no PVPs are seen temporally (B), indicating that these PVPs are multifocal in origin. D, A regressed hyaloid vessel within both the Cloquet canal and a PVP (arrows) is seen by swept-source optical coherence tomography in the eye of a 5-year-old boy.

9 years, a PVP was present in 16 eyes (49%) and a crack in 20 eyes (61%). Nine eyes (56%) with a PVP also had a crack. Among eyes with both a PVP and a crack, 16 eyes (86%) had cracks connected to the PVP. Twenty-eight eyes (80%) with PVPs had a liquefied connection between the PVP and the Cloquet canal (Figure 1C-F). The connection to the Cloquet canal was identified in both the PVP and the crack (Figure 1B). In younger eyes, the PVP was wider horizontally than vertically, and all detectable cracks were wider horizontally than vertically. During the early phase of PVP development, several eyes had multifocal PVPs and cracks (**Figure 2**A-C) in the premacular vitreous. A high-density structure, which appeared to be a remnant of regressed hyaloid vessels and was connected to the Bergmeister papilla, was present temporally along the crack and wall of the PVP in several eyes (Figure 2D).

Discussion | Kishi and Shimizu[3] originally identified PVPs in eyes at autopsy and implied that development began with slight separation of the vitreous at about age 2 years, although the PVPs might include postmortem changes. The current in vivo study showed that a PVP is often absent at birth and is often present by about age 3 years. Interestingly, the crack in the formed vitreous also was observed as an initial change around age 2 years.

The PVP and posterior Cloquet canal, which are separated by a dishlike wall of vitreous,[4] were connected in most eyes of the current patients, even in eyes with a crack at an initial stage. Aqueous humor from the posterior Cloquet canal[5] may play a role in formation of the crack and PVP.

Almost all primary PVPs and cracks that occasionally developed multifocally and coexisted with remnants of hyaloid vessels were wider horizontally than vertically. Because ocular movement is usually dominant horizontally, horizontal shear stress might generate cracks in horizontally layered premacular vitreous,[6] in which remnants of hyaloid vessels may be related to the friability of the premacular vitreous. The vitreous and hyaloid vessels are symmetric along the anteroposterior axis during early development and become asymmetric after dominant growth of the temporoposterior region. Since the remnant, cracks, and PVPs were observed only temporally in the premacular vitreous, the asymmetric vitreous growth may contribute to the asymmetric location of these structures. Further study is needed to confirm our preliminary findings.

Tadashi Yokoi, MD, PhD
Naoki Toriyama, MD
Takahiro Yamane, MD, PhD
Yuri Nakayama, MD
Sachiko Nishina, MD, PhD
Noriyuki Azuma, MD, PhD

Author Affiliations: Department of Ophthalmology and Cell Biology, National Center for Child Health and Development, Tokyo, Japan (Yokoi, Toriyama, Yamane, Nakayama, Nishina, Azuma).

Corresponding Author: Dr Azuma, Department of Ophthalmology and Cell Biology, National Center for Child Health and Development, 2-10-1, Okura, Setagaya-ku, Tokyo 157-8535, Japan (azuma-n@ncchd.go.jp).

Published Online: June 13, 2013.
doi:10.1001/jamaophthalmol.2013.240.

Conflict of Interest Disclosures: None reported.

1. Kishi S, Hagimura N, Shimizu K. The role of the premacular liquefied pocket and premacular vitreous cortex in idiopathic macular hole development. *Am J Ophthalmol.* 1996;122(5):622-628.

2. Worst JG. Cisternal systems of the fully developed vitreous body in the young adult. *Trans Ophthalmol Soc U K.* 1977;97(4):550-554.

3. Kishi S, Shimizu K. Posterior precortical vitreous pocket. *Arch Ophthalmol.* 1990;108(7):979-982.

4. Shimada H, Hirose T, Yamamoto A, Nakashizuka H, Hattori T, Yuzawa M. Depiction of the vitreous pocket by optical coherence tomography. *Int Ophthalmol.* 2011;31(1):51-53.

5. Duke-Elder S. *System of Ophthalmology, Volume II: The Anatomy of the Visual System.* London, England: Henry Kimpton; 1961:303-304.

6. Agarwal A. Macular dysfunction caused by vitreous and vitreoretinal interface abnormalities. In: *Gass' Atlas of Macular Disease.* 5th ed. Elsevier Saunders; 2012:636.

Electroretinography combined with spectral domain optical coherence tomography to detect retinal damage in shaken baby syndrome

Yuri Nakayama, MD, Tadashi Yokoi, MD, PhD, Nishina Sachiko, MD, PhD, Makiko Okuyama, MD, PhD, and Noriyuki Azuma, MD, PhD

In order to correlate anatomical changes with visual function in shaken baby syndrome, we performed electroretinography and spectral domain optical coherence tomography on a 2-month-old girl and a 9-month-old girl after the retinal hemorrhages absorbed. Both patients had significant abnormalities in spectral domain optical coherence tomography images of the macular area. The amplitudes of the focal macular electroretinograms were more severely decreased than those of the full-field electroretinograms. Combining spectral domain coherence tomography with focal macular electroretinograms might better estimate the functional damage to the macula in patients with shaken baby syndrome.

Case 1

A 2-month-old otherwise healthy girl with convulsions and epileptic seizures was transferred to the Pediatric Intensive Care Unit at the National Center for Child's Health and Development, Tokyo, for evaluation. Computed tomography scan showed massive subdural hemorrhages from the anterior skull base to the parietal lobe, with diffuse brain edema and multiple brain contusions around the sylvian fissure. Fourteen hours after admission, an ophthalmologic examination showed bilateral multilayered retinal hemorrhages (Figure 1A). The diffuse and dense preretinal, intraretinal, and subhyaloidal hemorrhages were predominantly in the posterior pole but were obscured bilaterally by the vitreous hemorrhages. The intraretinal hemorrhages also extended to the peripheral area. The Suspected Child Abuse and Neglect team diagnosed the patient with shaken baby syndrome (SBS).

The retinal hemorrhages were absorbed completely after 6 months. During this period, we did not perform vitrectomy because the patient was comatose for 3 months as a result of the extensive cerebral injury. We confirmed that the retinal hemorrhages were symmetric and the posterior pole of the retina was observed clearly 4 months after the injury when she gradually recovered consciousness.

Two years after the first examination, the patient had mild mental retardation and cerebral palsy affected the lower legs. Right esotropia with latent nystagmus was confirmed when the left eye was covered. Fixation in the right eye was not confirmed. An aversion response was obvious in the right eye when the left eye was covered. The visual acuity based on a Teller Acuity Card examination showed 0.31 cycles per degree in the left eye.

The complete ocular examination under general anesthesia showed wide chorioretinal degeneration and epiretinal membrane around the arcade vessels in both eyes. The optic disk was pale and fundus examination did not confirm the macular ring reflex in the right eye (Figure 1B). Fluorescein angiography showed a diffuse window defect, particularly along the arcade vessels. Some foveal vascular structures disappeared and the avascular area was wider than normal bilaterally (Figure 1C). There was a relatively wide avascular area from the midperiphery to the anterior nasally and temporally in both eyes (Figure 1D). Spectral domain optical coherence tomography (SD-OCT) images showed focal posterior vitreous separation and marked disruption of the retinal layers in the macula bilaterally. All electroretinography (ERG) components were smaller bilaterally in this case than in the age-matched normal control, and the ERG responses in the right eye were lower than in the left eye (Figure 2). The bright flash response was smaller, but a negative b-wave was seen and the a-wave was preserved bilaterally. A 30 Hz flicker response was significantly reduced in the right eye. The focal macular electroretinogram (fmERG) responses in the right eye were almost flat and nonrecordable, but the responses in the left eye showed an adequate waveform, although with a lower amplitude compared with the control.

Case 2

A 9-month-old girl was referred to the National Center for Child's Health and Development for evaluation of the ocular sequelae of SBS. She had sustained bilateral vitreous and subhyaloid hemorrhages 1 month before. A magnetic resonance imaging scan showed a left frontal subdural hemorrhage and a left palpebral subdural hemorrhage. The latter was assumed to be relatively old because the magnetic resonance imaging signal was lower

Author affiliation: National Center for Child's Health and Development, Tokyo, Japan
Submitted November 25, 2012.
Revision accepted February 23, 2013.
Published online July 17, 2013.
Correspondence: Yuri Nakayama, MD, 2-10-1 Okura, Setagaya-ku, Tokyo, Japan (email: nakayama-y@ncchd.go.jp).
J AAPOS 2013;17:411-413.

1091-8531/$36.00
http://dx.doi.org/10.1016/j.jaapos.2013.02.011

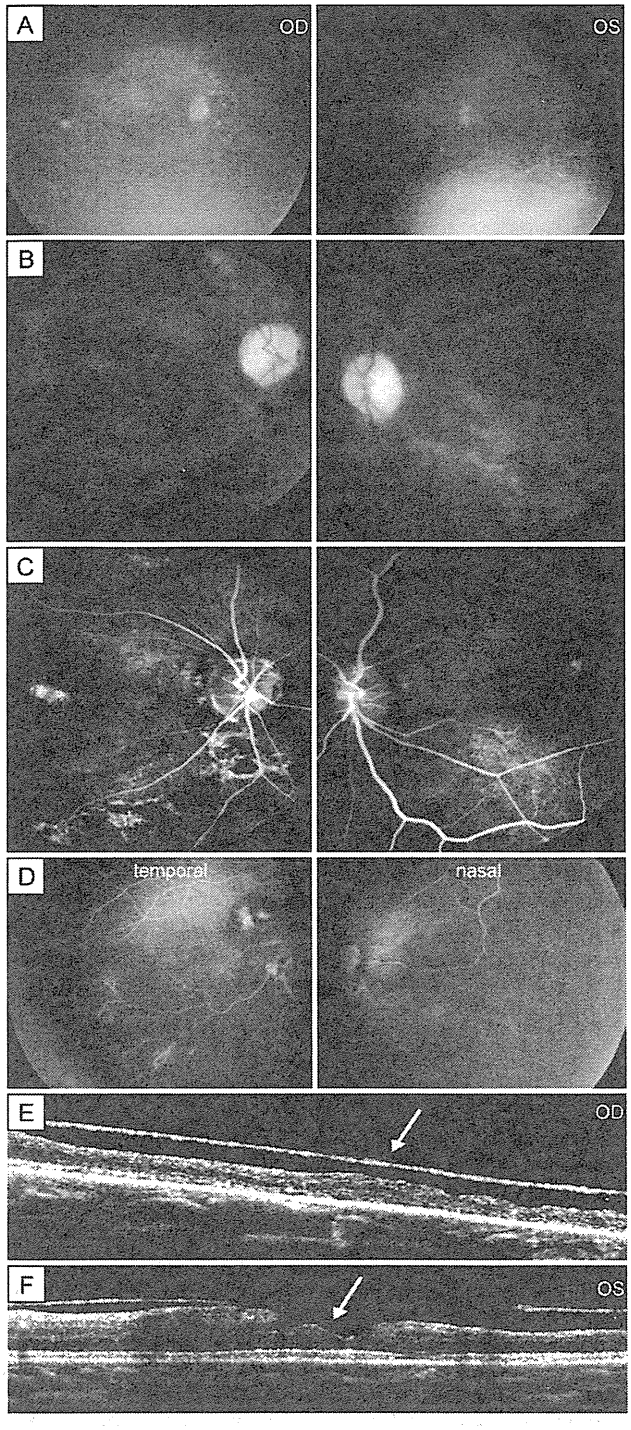

FIG 1. A, A RetCam photograph of an infant (Case 1) with shaken baby syndrome showing dense preretinal, intraretinal, and subhyaloidal hemorrhages predominantly in the posterior pole, obscured bilaterally by vitreous hemorrhages. B, Two years after the injury, marked chorioretinal degeneration with an epiretinal membrane in the posterior pole is seen bilaterally; the optic nerve is pale, and no macular reflux is seen in the right eye. C, Fluorescein angiography (FA) showing a diffuse window defect in the posterior pole bilaterally; loss of the vascular structures is confirmed in the fovea. D, A RetCam FA image showing an area of nonperfusion in the peripheral area nasally and temporally. E-F, SD-OCT images of the right eye and the left eye showing a focal posterior vitreous separation and a markedly disrupted retinal layer in the fovea bilaterally (arrows), especially in the right eye. *OD*, right eye; *OS*, left eye.

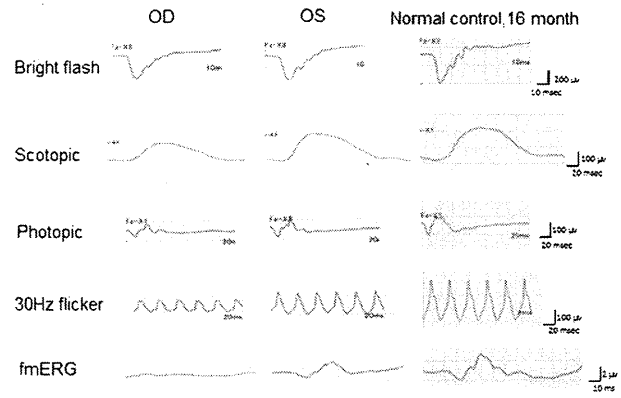

FIG 2. Full-field electroretinograms (ERGs) and focal macular electroretinograms (fmERGs) recorded from Case 1 and a normal control. All ERG components are smaller bilaterally in Case 1 than in the normal control, especially the 30 Hz flicker and fmERG responses. The fmERG shows a nonrecordable wave in the right eye and mildly reduced amplitude in the left eye. *OD*, right eye; *OS*, left eye.

than that of the hemorrhages in the frontal lobe. During our first examination, the vitreous and subhyaloid hemorrhages had almost resolved bilaterally. She could fix and follow, and was orthophoric; there was no nystagmus. Complete ophthalmologic examinations were performed subsequently.

Bilateral indirect fundus examination identified white, elevated rings outside the major vascular arcades around the macula that were consistent with perimacular folds (Figure 3A). Fluorescein angiography showed no distinct abnormal findings in the architecture of the foveal vessels using a fundus camera, and imaging showed no obvious avascular areas bilaterally.

SD-OCT images showed a wide perimacular focal posterior vitreous separation (Figure 3C, D). The foveal structures were mostly spared and the inner segment/outer segment line was seen clearly bilaterally. All full-field ERGs were smaller bilaterally in this case than in the normal control and a negative b-wave was nonrecordable (Figure 4). The waves in the right eye generally were slightly lower than those in the left eye, which was particularly obvious for the 30 Hz flicker response. However, while the fmERGs were recorded, the amplitude in the right eye decreased markedly. We did not perform vitrectomy, because we did not confirm retinal traction and the retinal hemorrhages mostly absorbed spontaneously.

After 4 months, at 10 month of age, her visual acuity measured using the Teller Acuity Cards in the right eye was 0.84 cycles per degree and in the left eye was 1.6 cycles per degree. No strabismus, nystagmus, or developmental delays were observed.

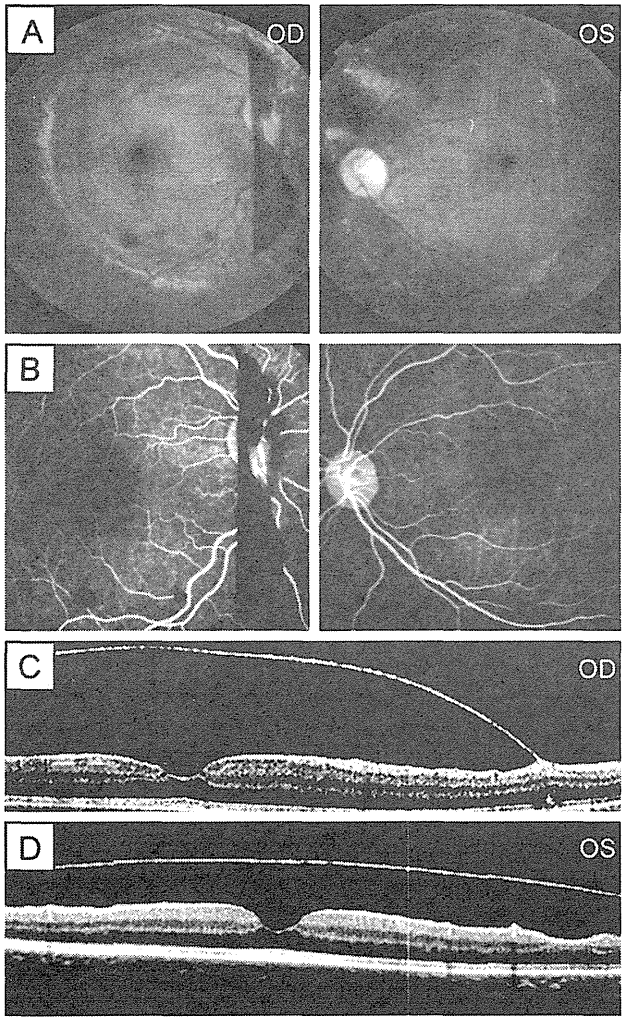

FIG 3. Fundus photograph and FA of an infant (Case 2) with bilateral SBS. A-B, Residual subhyaloid and retinal hemorrhages are confirmed in the right eye; the macula appears normal in both eyes. C-D, The foveal structures are mostly unaffected, as seen on SD-OCT images, although wide perimacular focal posterior vitreous separations are seen bilaterally. *OD*, right eye; *OS*, left eye.

Discussion

The present study investigated the correlation between the morphologic changes and fmERGs in 2 cases of SBS to predict the visual prognosis. We found that severe disruption of the retinal layers on SD-OCT might be better correlated with lower amplitude of the fmERGs than the amplitudes of the full-field ERGs; however, this study was too small to be certain that this is a true association. Previous ERG studies in patients with SBS have suggested that the inner retinal layer was primarily responsible for visual loss because a reduced b-wave and a relatively well-preserved a-wave were reported on full-field ERG.[1,2] fmERG is a noninvasive technique to objectively assess the neural activities of the macular area.[3] The correlation between the fmERG amplitude and macular volume by optical coherence tomography in retinitis pigmentosa[4] and visual acuity in age-related macular degeneration[5] has been previously reported. Performing fmERGs might facilitate further understanding of the macular functional damage in SBS.

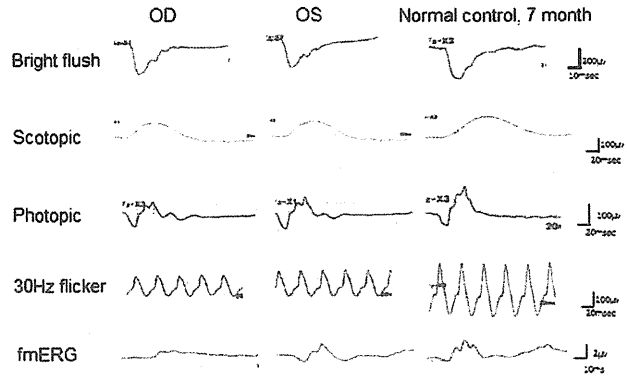

FIG 4. Full-field ERGs and fmERGs recorded from Case 2 and a normal control. All ERG components are smaller bilaterally in Case 2 than in the normal control, especially the 30 Hz flicker and fmERG responses. The fmERGs show waves with markedly lower amplitudes in the right eye and mildly reduced amplitudes in the left eye.

References

1. Greenwald MJ, Weiss A, Oesterle CS, Friendly DS. Traumatic retinoschisis in battered babies. Ophthalmology 1986;93:618-25.
2. Fishman CD, Dasher WB, Lambert SR. Electroretinographic findings in infants with the shaken baby syndrome. J Pediatr Ophthalmol Strabismus 1998;35:22-6.
3. Miyake Y, Shinoyama N, Horiguchi M, Ota I. Asymmmetry of focal ERG in human macular region. Invest Ophthalmol Vis Sci 1989;30: 1743-9.
4. Sugita T, Kondo M, Piao C. Macular volume and focal macular electroretinogram in patients with retinitis pigmentosa. Invest Ophthalmol Vis Sci 2008;49:3551-8.
5. Nishibara H, Kondo M, Ishikawa K. Focal macular electroretinograms in eyes with wet-type age-related macular degeneration. Invest Ophthalmol Vis Sci 2008;49:3121-5.

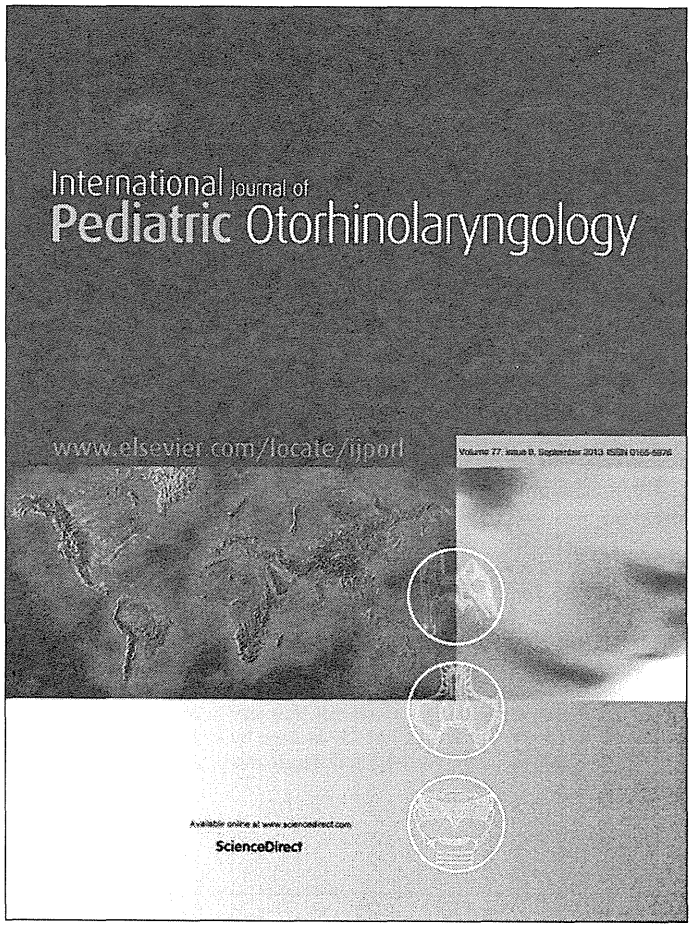

International Journal of Pediatric Otorhinolaryngology 77 (2013) 1596–1600

Contents lists available at SciVerse ScienceDirect

International Journal of Pediatric Otorhinolaryngology

journal homepage: www.elsevier.com/locate/ijporl

Case report

Gorham–Stout syndrome affecting the temporal bone with cerebrospinal fluid leakage

Noriko Morimoto [a,*], Hideki Ogiwara [b], Osamu Miyazaki [c], Masayuki Kitamuara [c], Sachiko Nishina [d], Atsuko Nakazawa [e], Takanobu Maekawa [f], Nobuhito Morota [b]

[a] Department of Otolaryngology, National Center for Child Health and Development, Tokyo, Japan
[b] Department of Neurosurgery, National Center for Child Health and Development, Tokyo, Japan
[c] Department of Radiology, National Center for Child Health and Development, Tokyo, Japan
[d] Department of Ophthalmology, National Center for Child Health and Development, Tokyo, Japan
[e] Department of Pathology, National Center for Child Health and Development, Tokyo, Japan
[f] Department of Pediatrics, National Center for Child Health and Development, Tokyo, Japan

ARTICLE INFO

Article history:
Received 30 April 2013
Accepted 2 June 2013
Available online 2 July 2013

Keywords:
CSF leak
Petrous apex
Lymphovascular proliferation
Interferon-α2
Proplanolol
VEGF

ABSTRACT

Gorham–Stout syndrome is a rare disorder characterized by progressive osteolysis that leads to the disappearance of bone. Lymphvascular proliferation causes the local destruction of bony tissue. Owing to the low incidence of this syndrome, little is known about its etiology or treatment. We present an 11-year-old girl with Gorham–Stout syndrome that involved right petrous apex in temporal bone and upper clivus, which cause intracranial pressure increase and cerebrospinal fluid (CSF) leakage. The patient required surgical repair of CSF leakage by extradural middle fossa approach with temporal fascia flap. Combined treatment with interferon and propranolol prevented the progression of osteolysis.

1. Introduction

Gorham–Stout syndrome is a rare disorder that is also known as "vanishing", "disappearing" bone disease because bony lymphangiomatosis results in progressive osteolysis. One or more bones affected by invasive changes such as chylothorax and lymphovascular proliferation in the adjacent soft tissue.

Recent reviews of the literature have identified more than 200 reported cases, with most patients presenting in childhood. Any part of the skeleton can be involved, with the most common sites being the cranium, shoulders, and pelvic girdle. The etiology is unknown and the symptoms depend on the affected sites. Multiple skeletal lesions due to lymphangiomatosis involve the head and neck in 20% of patients. However, there are only 3 reported cases of cerebrospinal fluid (CSF) leakage secondary to lymphangiomatosis of the temporal bone [1–3] and both patients had a history of meningitis. Here we present a patient with lymphangiomatosis in the apex of the petrous temporal bone, who presented with hearing loss, tinnitus, and nausea secondary to elevated intracranial pressure and CSF leakage.

2. Case report

An 11-year-old girl without remarkable family history had previously been healthy. She was referred to our clinic with vertigo, headache, and pulsatile tinnitus. She had suddenly heard a faint rupturing sound, and then had suffered from nausea and headache for 1 week. Although the nausea had gradually subsided, her headache was persistent.

Otoscopic examination showed no abnormal findings in both ear. Pure tone audiometry revealed mild conductive hearing loss at low frequencies (125, 250, and 500 Hz), with a normal threshold over 1 kHz. Tympanometry showed that both ears were type A. A normal response was obtained when distortion products of otoacoustic emissions (DPOAE) were tested.

Papilledema was found in both eyes, indicating elevation of intracranial pressure or optic chiasm compression. There were no abnormalities in her visual acuities, visual fields, ocular alignment, extraocular movements, and binocular function.

* Corresponding author at: Department of Otolaryngology, National Center for Child Health and Development, Okura 2-10-1, Setagaya, Tokyo 157-8535, Japan. Tel.: +81 3 3416 0181; fax: +81 3 5494 7909.
E-mail address: morimoto-n@ncchd.go.jp (N. Morimoto).

0165-5876/$ – see front matter © 2013 Elsevier Ireland Ltd. All rights reserved.
http://dx.doi.org/10.1016/j.ijporl.2013.06.004